Astron. Astrophys. 320, 831–839 (1997)

ASTRONOMY AND ASTROPHYSICS

# ROSAT and AB Doradus: the first five years

**M. Kürster[1,2], J.H.M.M. Schmitt[1], G. Cutispoto[3], and K. Dennerl[1]**

[1] Max-Planck-Institut für extraterrestrische Physik, Giessenbachstr., D-85740 Garching, Germany
[2] Institut für Astronomie, Universität Wien, Türkenschanzstr. 17, A-1180 Wien, Austria (kurster@astro.ast.univie.ac.at)
[3] Osservatorio Astrofisico, Viale A. Doria 6, I-95125 Catania, Italy

Received 21 May 1996 / Accepted 9 October 1996

**Abstract.** Five and a half years of data from an extensive ROSAT X-ray monitoring program devoted to the young K-star AB Dor are presented. Begun in mid-1990, this program is aimed at the study of the long-term behaviour of coronal flux levels in this very active star. We compare the X-ray data with 17 years of V-band brightness monitoring that shows a 10-year decline between 1978 and 1989 and a subsequent rise phase. In contrast, the X-ray flux, which is very variable on time scales of minutes to weeks, exhibits no pronounced long-term trend over the 5 1/2 years of the program. This supports the concept of a saturated corona. Making use of the ROSAT all-sky survey data and data from the most extensive among the available pointed observations we also discuss the short-term variablity in relation to the rotational time scale. We find evidence for a partial rotational modulation of the X-ray flux implying structural inhomogeneities in this saturated corona.

**Key words:** stars: coronae – stars: activity – stars: rotation – stars: individual: AB Dor – X-rays: stars

## 1. Introduction

Coronal X-ray emission is an excellent tracer of stellar activity. The solar soft X-ray luminosity as measured by the YOHKOH SXT varies by a factor of $\approx$ 20 (Acton 1996) following the Sun's activity cycle. On the contrary, variations of the solar visual brightness are of the order of 0.1%. If the Sun were at stellar distances, it would be difficult to observe (from the ground) any variability of its disk integrated visual brightness, whereas the cyclic variation of its X-ray luminosity would be easily detectable.

Rapidly rotating pre-main sequence stars or RS CVn-type binaries have X-ray luminosities exceeding the Sun's X-ray output by 3 orders of magnitude. While long-term changes of the visual brightness by a few tenths of a magnitude are common in these objects (e.g. Cutispoto 1995), little is known about the long-term behaviour of their X-ray flux on time scales of several years. In this paper we report on an extensive long-term X-ray study of the active young K-star AB Dor (= HD 36705) which is a rapidly rotating pre-main sequence K0V star with a rotation period of 12.35 h and a projected rotational velocity $v \sin i$ = 93 km sec$^{-1}$ (Kürster et al. 1994). Individual one-epoch X-ray and EUV observations of AB Dor were previously made with the *Einstein* (Pakull 1981; Vilhu & Linksy 1987), EXOSAT (Cameron et al. 1988), GINGA (Vilhu et al. 1993), ASCA (White et al. 1995), and EUVE (Ruciński et al. 1995) satellites.

*Send offprint requests to*: M. Kürster

## 2. Data acquisition and reduction

The X-ray observations presented here were carried out with the ROSAT satellite (Trümper 1983) using both the PSPC (Pfeffermann et al. 1987) and HRI (David et al. 1993) detectors which both operate in the energy range of 0.1 − 2.4 keV. We produced background subtracted light curves corrected for vignetting and deadtime using the EXSAS software (Zimmermann et al. 1994).

## 3. Long-term photospheric vs. coronal variability

### *3.1. V-band data*

In the 10 years from 1978 to 1988 AB Dor's average visual brightness declined perpetually by $\approx 0\overset{\mathrm{m}}{.}2$; in 1989 the reverse trend began, and a plateau was reached in recent years. This brightness evolution is shown in Fig. 1, adapted from Kürster et al. (1994) and supplemented with data by Anders (1994), Bos (1994a,b), Bos et al. (1995a,b; we have excluded an obvious white light flare from the data of Oct 22, 1995), Unruh et al. (1995), and Cutispoto (unpublished). As of now it is unclear whether this variability is cyclic or irregular.

### *3.2. X-ray data*

#### 3.2.1. The long-term ROSAT light curve

In order to study the long-term evolution of the coronal X-ray emission in an active star a still ongoing ROSAT monitoring program on AB Dor was begun in mid-1990. AB Dor was selected, because it is a bright X-ray source located near the southern

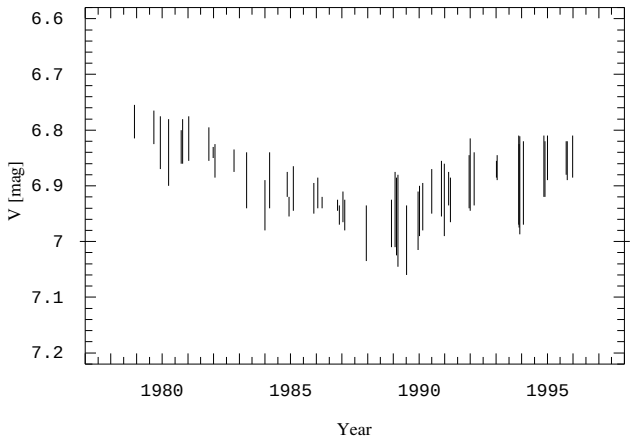


**Fig. 1.** AB Dor's long-term V-band brightness evolution. Each vertical bar represents the range of observed short-term variability due to spot induced rotational modulation.

**Table 1.** Results from the search for a long-term trend in the X-ray data. FAP is the false alarm probability obtained from the assumption of a normal distribution of the deviations of the count rate data from the fit curve (ND) and from bootstrapping the observed distribution of the measurements (BS).

| data set | best fit slope [cts sec$^{-1}$ yr$^{-1}$] | increase per year [%] | FAP ND [%] | FAP BS [%] |
|---|---|---|---|---|
| PSPC | $0.22 \pm 0.16$ (PSPC) | $3.3 \pm 2.4$ | 8.2 | 9.1 |
| HRI | $0.089 \pm 0.038$ (HRI) | $4.4 \pm 1.9$ | 0.93 | 0.44 |
| PSPC+HRI | $0.11 \pm 0.11$ (PSPC) | $1.6 \pm 1.7$ | 17. | 8.8 |
| | $0.033 \pm 0.034$ (HRI) | | | |

ecliptic pole and therefore visible to ROSAT at all times. It was also chosen because of its pronounced V-band variability and because it resembles a young Sun. In the monitoring program AB Dor is observed once per month for $1 - 1.5$ ksec. We complemented the data set by ROSAT all-sky survey data (see also Kürster et al. 1992) and by a number of pointed observations of longer duration (cf. Kürster & Dennerl 1993).

Fig. 2 shows the temporal behaviour of the soft X-ray count rate as observed between mid-1990 and late 1995. PSPC data are plotted as circles (or triangles if obtained during the all-sky survey); HRI data are depicted by crosses. Data from pointed observations (both PSPC and HRI) were combined into one bin per satellite observing slot (typically $1 - 1.5$ ksec per 96 min satellite orbit) whereas data from the all-sky survey were binned into one bin per day. (Note that different binning was used for the short-term studies in Sect. 4.) The systematically lower HRI count rates result from the reduced sensitivity of the HRI and do not reflect any stellar property. In 1994 the PSPC became unavailable for this program which has since then been continued exclusively with the HRI.

Strong short-term variability is evident – the statistical error bars are mostly smaller than the plot symbols. The majority of our measurements are short snapshots which do not cover the whole range of the large short-term variability present at any given instant (cf. Sect. 4). The formal best fitting straight lines (least squares fits) to both the observed PSPC and the HRI count rates are plotted as solid lines. Both fits yield very small positive slopes, viz. $0.22 \pm 0.16$ cts sec$^{-1}$ yr$^{-1}$ for the PSPC, corresponding to a flux increase of $3.3\% \pm 2.4\%$ per year, and $0.089 \pm 0.038$ cts sec$^{-1}$ yr$^{-1}$ for the HRI, equivalent to a yearly flux increase of $4.4\% \pm 1.9\%$. Also shown in Fig. 2 is a simultaneous linear fit to both data sets (dashed lines) made under the constraint that both trends are correlated such that the ratio of the PSPC and HRI count rates (and hence the ratio of the slopes) is a constant $C$. Lacking a comprehensive comparative study of the HRI and PSPC fluxes of coronally active stars we determined $C$ also by the fit finding $C = 3.2$. In this case we obtain an even smaller slope of $0.11 \pm 0.11$ cts sec$^{-1}$ yr$^{-1}$ for the PSPC (i.e. $0.033 \pm 0.034$ cts sec$^{-1}$ yr$^{-1}$ for the HRI) corresponding to a yearly flux increase of only $1.6\% \pm 1.7\%$.

The given errors of the obtained slopes are $1\sigma$ errors determined under the assumption of normally distributed deviations of the count rate measurements from the fit curve (single-parameter 68% confidence intervals; i.e. treating other fit parameters as uninteresting; cf. Avni 1976). Using these errors we find a slope of zero to be within $1.4\sigma$, $2.4\sigma$, and $0.96\sigma$ of the formal best fit slope for the PSPC, HRI, and combined PSPC+HRI data, respectively. Conversely, the probability that a positive slope as large as (or larger than) the observed one results merely from the measurement uncertainties (false alarm or chance probability) is 8.2%, 0.93%, and 17%, for the PSPC, HRI, and combined PSPC+HRI data, respectively.

#### 3.2.2. Trend analysis via bootstrap

As the assumption of normally distributed measurement deviations (from the model curve) is not strictly valid for our data set(s) we adopted a bootstrap approach (using the observed distribution of the count rate measurements) to perform an independent determination of the significance of the small positive slopes obtained for both the PSPC and HRI data sets individually as well as for the combined data set. The bootstrap method (Efron 1979) was first applied to astronomical data by Barrow et al. (1984) and by Schmitt (1985) as a 'bootstrap resampling technique.' The variant we use in this paper, a 'bootstrap randomization technique' (cf. Bieber et al. 1990), can be described as follows.

In order to investigate the chance probability that a slope as large as the observed one (or larger) is inferred from the given distribution of count rates and observing times present in our data set(s) we ran a Monte-Carlo simulation by making linear fits to simulated data sets constructed in the following fashion. Retaining the observing times we randomly redistributed the observed count rates amongst the times (cf. Murdoch et al. 1993). In all three data sets (PSPC, HRI, combined PSPC+HRI) the number of possible permutations ($n!$) is too large for a com-

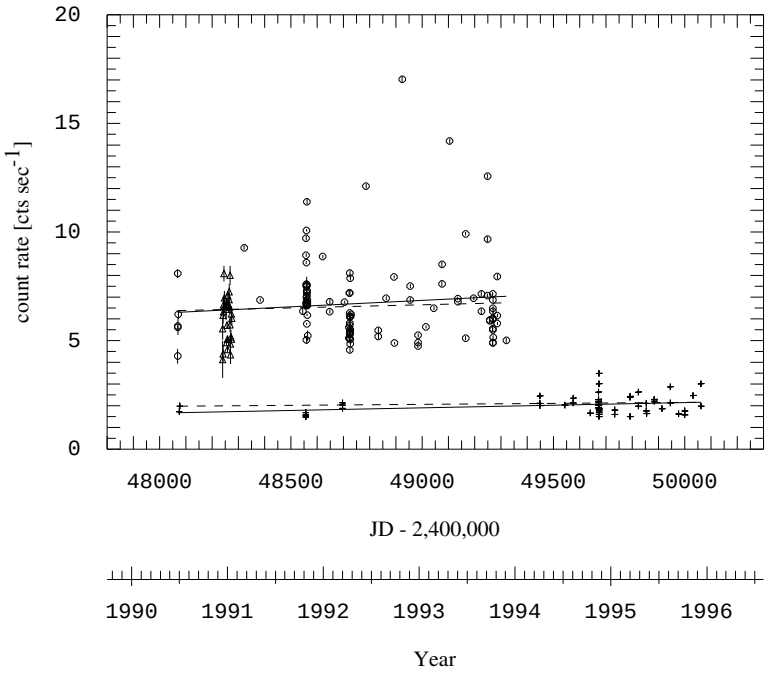


**Fig. 2.** The ROSAT monitoring observations of AB Dor. PSPC measurements are represented by circles (pointed observations) or triangles (all-sky survey). Data from the less sensitive HRI are depicted by crosses. Linear least squares fits to both the PSPC and HRI data are shown as solid lines. Dashed lines represent a combined fit to both data sets (see text).

plete evaluation of the pertaining distribution of slopes so that we confined ourselves to approximating the true distribution by a subset of 10,000 randomly chosen sequences. For the PSPC data we found that in 9.1% of the cases slopes as large as the observed one (or larger) are obtained by pure chance, whereas for the HRI data this is found only in 0.44% of the cases. This may be considered a marginal detection of a positive slope in the HRI data. However, when the combined fits to the PSPC+HRI data sets are used we find a chance probability of 8.8% to obtain a slope (at least) as large as the observed one, comparable to that of the pure PSPC data set. Table 1 summarizes these results.

Consequently, no significant long-term trend in AB Dor's X-ray flux can be inferred from the ROSAT measurements at present. If anything, the HRI data point at a possible long-term increase which, however, is certainly not comparable to the cyclic soft X-ray variability of the Sun. In the time interval for which ROSAT data are available (after 1990.5) also the V-band flux shows much less systematic change than in previous years. For this reason it is premature to assess any possible correlation (or lack thereof) between AB Dor's average X-ray flux and V-band brightness.

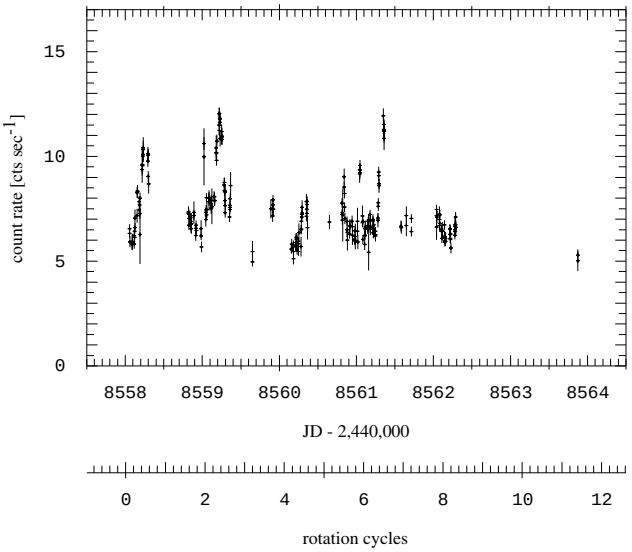


**Fig. 3.** X-ray light curve from a 46 ksec ROSAT PSPC pointing on AB Dor plotted vs. Julian day and the rotational cycle.

The lack of any clear evolution of the X-ray flux supports the concept that the coronae of very active stars are saturated. Saturation of the chromospheric and coronal emission levels of late-type stars was found by Vilhu (1984) in a sample of F, G, and K-stars of different rotational periods. It occurs at large values of Vilhu's 'activity parameter' (a measure of the ratio of convective turnover time and rotation period similar to the inverse Rossby number; see also Vilhu & Walter 1987) and was interpreted as a consequence of the 'filling factor' appoaching unity. (The 'filling factor' is a simplifying measure of the fraction of stellar surface covered with active regions; in general, coronal emissivity depends on the emitting volume and on the square of the plasma density.)

The concept of saturation is best illustrated by the observational fact that the most rapidly rotating late-type stars in young stellar clusters such as the Pleiades (i.e. in samples of stars of equal age) have equal X-ray-to-bolometric luminosity ratios $L_{\rm x}/L_{\rm bol}$. Stauffer et al. (1994) found $L_{\rm x}/L_{\rm bol}$ to increase with the projected rotational velocity $v \sin i$ for Pleiades G and K-stars up to $v \sin i$ = 20 km sec$^{-1}$ and to be constant beyond. Indications that AB Dor is at the same evolutionary stage as the Pleiades come from the strength of its LiI $\lambda$6707 absorption

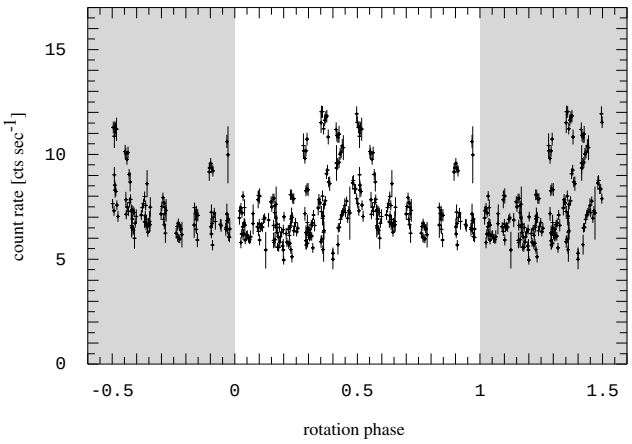


**Fig. 4.** X-ray data of Fig. 3 folded with the rotational period and plotted vs. the phase interval $[-0.5, 1.5]$. Every data point is plotted twice (repeated in the shaded area).

line from which an age of $10^6 - 3 \times 10^7$ years was estimated (Ruciński 1982, 1985, Vilhu et al. 1987). This is further supported by AB Dor's membership in the Pleiades moving group (Innis et al. 1986). For AB Dor we determine an average value of $\log(L_x/L_{bol}) = -3.05$ which compares well with the rapid rotators among the Pleiades G and K-stars (Stauffer et al. 1994). A saturated level of AB Dor's transition region emission was already reported by Vilhu (1984; "note added in proof.")

## 4. Short-term coronal variability

### *4.1. The extensive pointed observation of Oct/Nov 1991*

#### 4.1.1. The Oct/Nov 1991 ROSAT light curve

Out of the wealth of ROSAT data of AB Dor a 46 ksec pointing carried out within 6 days (Oct 28-Nov 03, 1991) is best suited to study short-term variability. Fig. 3 shows the X-ray light curve of this observation. The data were binned into 200 sec intervals resulting in 280 time bins of which 163 were 'complete bins' with 200 sec exposure and 117 were 'uncomplete bins' covering shorter exposure times between 6 and 199 sec. Fig. 4 shows the same data folded with the ephemeris by Innis et al. (1988) $HJD\ 2,444,296.575 + 0.51479 \times E$. Rotational modulation appears to be present to some extent, but with substantial erratic fluctuations superimposed. Assuming the latter to be caused by flares, one can expect to find a well defined, smoothly varying lower envelope to the data points representing the flux from the quiescent corona. This can actually be seen in Fig 4, and the lower envelope is found to reach a maximum at phase $\phi = 0.5$. Most of the major flares occur near the same phase supporting the hypothesis that indeed the more active hemisphere is in view.

#### 4.1.2. Periodogram analysis

In order to test the statistical significance of our claim that a fraction of the coronal emission is rotationally modulated, an estimator is required for the chance probability that the X-ray flux is found to vary with the *known* rotation period. We shall, however, adopt a much more conservative point of departure and set our goal as trying to *find* the rotation period of AB Dor in a timing analysis of the data. If successful, additional credibility will be lent to our claim.

For this purpose we ran a period search analysis using the periodogram introduced by Scargle (1982) which is a variant of the 'classical' periodogram (based on discrete Fourier transforms) adapted for unevenly spaced data. The Scargle periodogram does not make use of the individual measurement errors (resulting from Poisson statistics), which in fact are unrelated to the observed short-term fluctuations in our data set; instead it uses the absolute variance of the data for probability estimates of possible periodicities. In order to base our analysis on data points of equal weight we constrained the data set by using only the 163 data points of the maximum bin size of 200 sec. We searched the total accessible frequency interval ranging from 1 cycle per total time baseline $T$ of the data $f_{min} = T^{-1}$ up to the Nyquist freqency $f_{max} = (2\Delta t)^{-1}$, where $\Delta t$ is the minimum step size between individual measurements. For our 'complete bins' data subset $T = 4.0$ day and $\Delta t = 200$ sec. The observed periodogram power can then be related to a probability for the detection of a spurious period (the false alarm probability) in the way described in the Appendix.

Fig. 5 shows the resulting periodogram; for display purposes we show only the more interesting frequency range of $0.25 - 10.0$ day$^{-1}$ corresponding to a period range of $0.1 - 4.0$ day. A number of highly significant peaks are present one of which (the third strongest) is near the rotation period of 0.51479 day reaching a false alarm probability (FAP) of $< 1 \times 10^{-4}$ at peak maximum and $6.3 \times 10^{-4}$ at the exact value of the rotation period (see also Table 2). The first harmonic (at 0.5 $P_{rot}$) also shows up at the $FAP \approx 0.1\%$ level. We will discuss the meaning of the other periodogram peaks below.

Having found a high probability for the presence of the rotation period in the data, we can now leave our conservative point of departure and proceed to estimate the chance probability for a signal at the *a priori known* value of the rotation period. For normally distributed errors this chance probability is given by $e^{-z}$, where $z$ is the observed height of the pertaining periodogram peak (Scargle 1982; Horne & Baliunas 1986; see also Appendix). We will call it the 'single frequency false alarm probability' (SFP). We find a very significant signal at $P_{rot}$ with a small value of $SFP = 1.1 \times 10^{-6}$ quantifying what is seen in Fig. 5. At peak maximum $SFP = 1.8 \times 10^{-8}$.

As it was our original goal to demonstrate that the 'quiescent emission' shows partial rotational modulation we repeated the periodogram analysis for the subset of data with a count rate $< 8.0$ cts sec$^{-1}$ trying to exclude most of the flaring emission. This further reduced the number of data points of this 'quiescent' data set to 122. The resulting periodogram is shown in Fig. 6. Again the third highest peak is found near the rotation period, closer than in the previous case, but at a lower significance level. Peak maximum and the power value at $P_{rot}$ are at $FAP = 3.6\%$ and 6.0%, and $SFP = 2.4 \times 10^{-5}$ and $3.9 \times 10^{-5}$, respectively

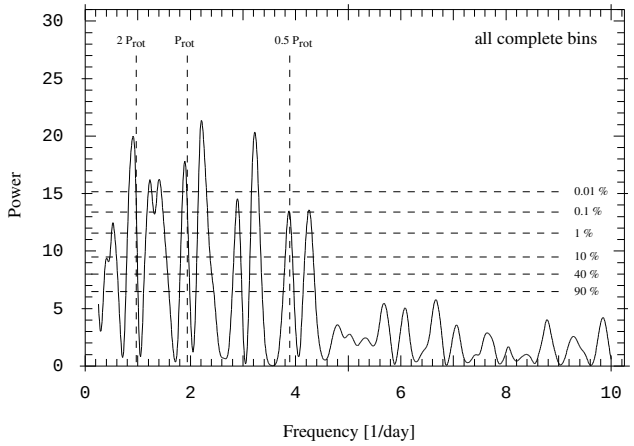


**Fig. 5.** Periodogram for the Oct/Nov 1991 poining data of AB Dor. Only complete time bins with 200 sec exposure time were used. Vertical dashed lines indicate period values of 0.5, 1, and 2 times the rotation period. Horizontal dashed lines give the false alarm probability levels.

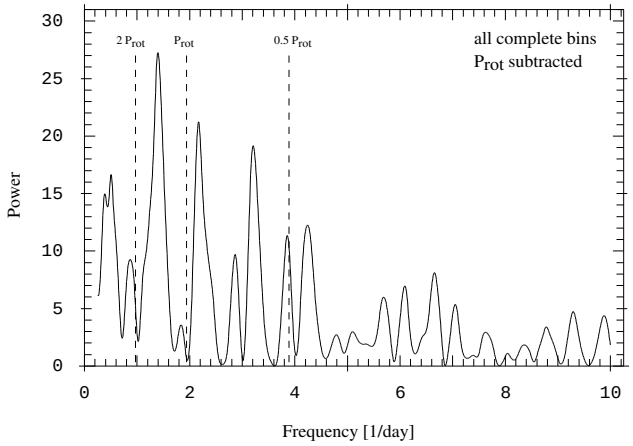


**Fig. 7.** Periodogram of the data set used for Fig. 5 (all complete 200 sec bins), but after subtraction of the best-fit sine wave with a period equal to AB Dor's rotation period $P$ = 0.51479 day. Note the artificially produced zero power at $P_{\rm rot}$.

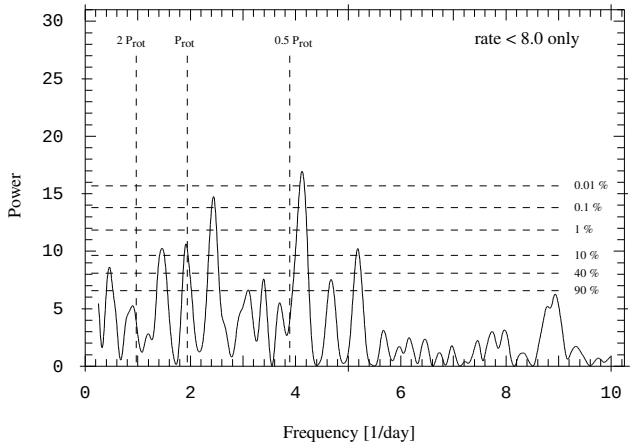


**Fig. 6.** Periodogram for the Oct/Nov 1991 poining data of AB Dor as in Fig. 5, but only for data with a count rate $< 0.8$ cts sec$^{-1}$. Vertical dashed lines indicate period values of 0.5, 1, and 2 times the rotation period. Horizontal dashed lines give the false alarm probability levels.

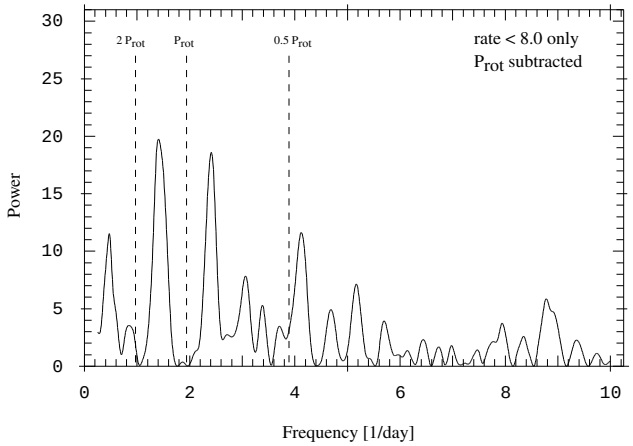


**Fig. 8.** Periodogram of the data set used for Fig. 6 (count rate $< 8.0$ cts sec$^{-1}$), but after subtraction of the best-fit sine wave with a period equal to AB Dor's rotation period $P$ = 0.51479 day. Note the artificially produced zero power at $P_{\rm rot}$.

(cf. Table 2). Obviously, removal of the flaring emission has led to a peak more consistent in frequency with the rotation period, but with reduced strength. This is in line with our above statement, that flares seem to preferentially occur on the more active hemisphere. As strong but episodic events of variability flares contribute substantially to the observed modulation, but do not follow a periodic behaviour equally precise as any purely geometrically caused modulation, since they can be recorded whenever the flaring region is in view. Therefore they will be seen to occur over a rather wide phase range (phases $\approx 0.3-0.65$ for the bulk of the flaring emission seen in Fig. 5).

We conclude that the quiescent emission of AB Dor in Oct/Nov 91 truely exhibited partial rotational modulation the degree of which can be estimated from the amplitude of a sine wave fit to the data with $P = P_{\rm rot}$. We find (semi-)amplitudes of $0.94 \pm 0.16$ cts sec$^{-1}$ for the 'complete bins' data set and $0.353 \pm 0.072$ cts sec$^{-1}$ for the 'quiescent' data set. (Errors are single-parameter $1\sigma$ errors valid for normally distributed deviations of the count rate measurements from the sine fit.) With mean levels of 7.363 cts sec$^{-1}$ and 6.814 cts sec$^{-1}$ these amplitudes correspond to a rotational modulation of $\pm 13\%$ and $\pm 5\%$ for the 'complete bins' data set and for the 'quiescent' data set, respectively.

We infer further evidence for partial rotational modulation from the existence of two unequally active hemispheres required to explain the observed phase distribution of flares. Here we assume that the same unequal hemispheres give rise to the modulation of the quiescent emission whose maximum falls within the phase range for the bulk of the flaring emission. We determined the phases of the maxima of least squares fit sine waves to both the 'complete bins' and the 'quiescent' data sets to be $0.482^{+0.054}_{-0.052}$ and $0.604^{+0.071}_{-0.068}$ phase units, respectively, showing

**Table 2.** Results from the search for rotational modulation in the Oct/Nov 1991 pointing data and in the first subset of the all-sky survey data. The Scargle power, the theoretical SFP as well as the SFP and FAP determined from the bootstrap (BS) analysis are listed for the rotation period and for the maximum of the nearest peak in the periodogram, respectively.

| Data set | Position | Power $z$ | theor. SFP $e^{-z}$ [%] | SFP (BS) [%] | FAP (BS) [%] |
|---|---|---|---|---|---|
| pointing | $P_{\rm rot}$ | 13.6 | 0.00011 | $\approx e^{-z}$ | 0.063 |
| 200 s bins | peak | 17.8 | 0.0000018 | $\approx e^{-z}$ | $< 0.010$ |
| pointing | $P_{\rm rot}$ | 10.1 | 0.0039 | $\approx e^{-z}$ | 6.0 |
| rate $< 8.0$ | peak | 10.6 | 0.0024 | $\approx e^{-z}$ | 3.6 |
| survey | $P_{\rm rot}$ | 5.4 | 0.47 | 0.089 | 18. |
| subset 1 | peak | 5.5 | 0.40 | 0.076 | 16. |

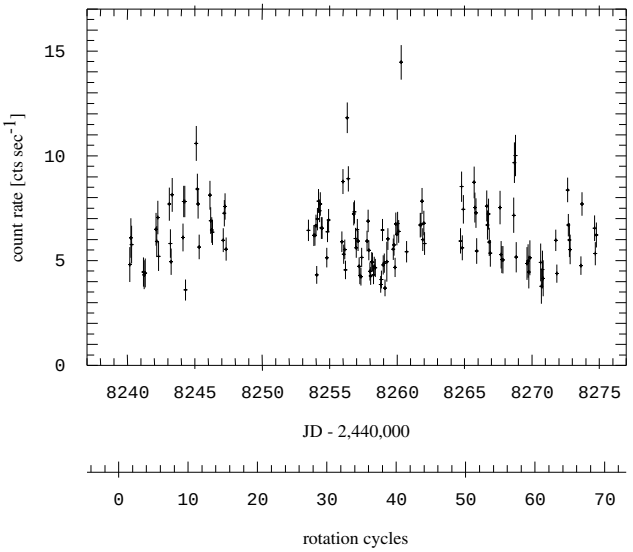


**Fig. 9.** ROSAT all-sky survey light curve of AB Dor plotted vs. Julian day and the rotational cycle (according to the ephemeris by Innis et al. 1988). As it is located near the southern ecliptic pole AB Dor was covered for 35 days or $\approx 70$ rotational cycles.

them to just coincide within their errors, if (as we have done in this case) the combined 68% confidence intervals for the 3 fit parameters of the sine waves are used.

What is the meaning of the other periodogram peaks? There are the following possibilities:

1. Other genuine periodicities exist in the data set.
2. There are episodic short-term trends that appear as periodic because of the short total time baseline over which they were observed.
3. The specific pattern of data gaps leads to substantial spectral leakage from the rotation frequency to other frequencies.

We have no means to exclude the first two possibilities, and in fact the second point could be used to argue that the observed power at the rotation period could also be the result of an episodic trend. This, of course, is a general problem in time series analysis based on a finite data string. The third point, however, can be tested by recomputing the periodogram after modifying the data set(s) by subtracting the best-fit sine wave(s) with $P = P_{\rm rot}$ from the observed data. The resulting periodogram for our 'complete bins' data set is shown in Fig. 7; Fig. 8 shows that of the 'quiescent' data set. Note the zero power at the rotation period in both figures. It should also be noted that the procedure leading to Figs. 7 and 8 is different from the usual way to estimate the amount of spectral leakage in a periodogram where the best-fit sine wave to the *highest* peak in the periodogram is subtracted. In our case (subtraction of the best-fit sine wave with $P = P_{\rm rot}$) the resulting periodogram may end up having peaks higher than those in the original periodogram.

When comparing Figs. 7 and 8 with the original periodograms Figs. 5 and 6 it becomes evident that essentially all of the high peaks survive (except at $P = P_{\rm rot}$ and $P = 2P_{\rm rot}$) so that they cannnot be the result of considerable spectral leakage from the rotational frequency. Therefore, their nature remains unclear.

### *4.2. The ROSAT all-sky survey data*

#### 4.2.1. The survey light curve

Fig. 9 shows the ROSAT all-sky survey PSPC light curve of AB Dor which was observed over 35 days. As a result of the scan mode used for the survey the source was covered once every 96 min for typically $20 - 30$ sec. The data were combined into one bin per satellite scan. Frequent data gaps are mostly due to detector switch-offs during satellite passage through the South Atlantic Anomaly.

The star is very variable exhibiting flaring activity as well as variability on time scales of a few hours. Three subsets of the all-sky survey data separated by the largest data gaps around JD 2,448,250 and 2,448,263 are displayed in Fig. 10a-c folded with the rotational period according to the ephemeris by Innis et al. (1988). These subsets comprise data obtained within 7, 9, and 10 days, respectively. Only in the first data subset phase-related variability appears to exist whereas the variability seen in the other two subsets is quite 'irregular,' i.e. attributable to low-level flaring and/or restructuring of coronal emission regions on short time scales.

#### 4.2.2. Periodogram analysis

As with the Oct/Nov 1991 pointing data we performed a periodogram analysis of the three subsets of the all-sky survey data in order to search for variability related to the rotational phase. For the three subsets of the survey data the limiting frequencies of the accessible frequency range are found as $f_{\rm min} = 1/T$ where $T = 7,\ 9$ and 10 days, and $f_{\rm min} = (2\Delta t)^{-1}$ where $\Delta t = 96$ min is the minimum sampling interval given by the orbital period of the ROSAT spacecraft.

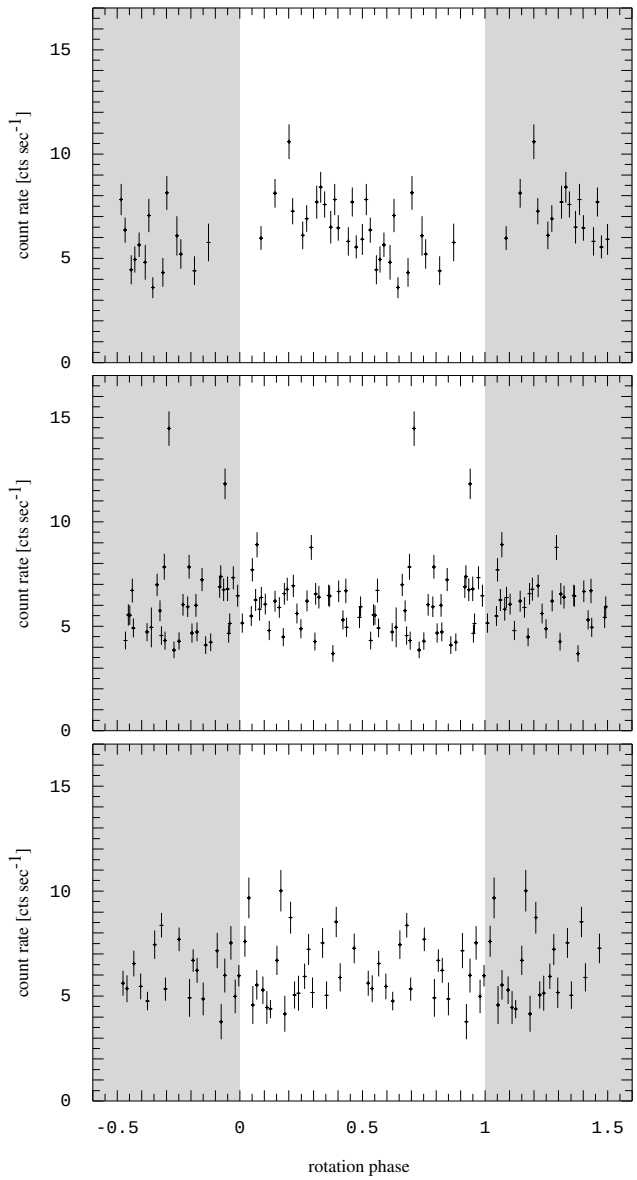


**Fig. 10.** Three subsets of the data shown in Fig. 9 folded with the rotation period and plotted vs. the phase interval $[-0.5, 1.5]$. Every data point is plotted twice (repeated in the shaded area). Top: JD $2,448,240 - 8,247$. Middle: JD $2,448,253 - 8,262$. Bottom: JD $2,448,264 - 8,274$.

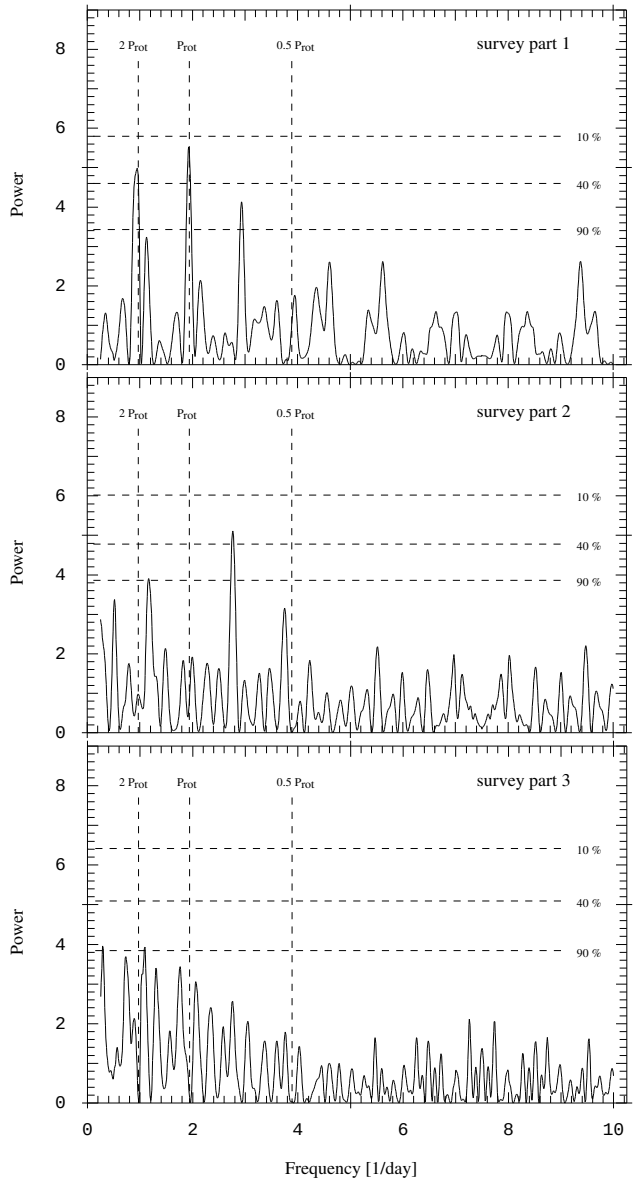


**Fig. 11.** Periodograms of the subsets of the all-sky survey data shown in Fig. 10a-c. Top: first subset JD $2,448,240 - 8,247$. Middle: second subset JD $2,448,253 - 8,262$. Bottom: third subset JD $2,448,264 - 8,274$. Dashed lines have the same meaning as in Figs. 5-8.

Fig. 11a-c shows the periodograms for the three data subsets of Fig. 10a-c. Again we show only the interesting frequency range $1/T \leq f \leq 10$ day$^{-1}$ corresponding to a period range of 0.1 day $\leq P \leq T$. Only the periodogram of the first data subset shows a peak at the rotation period with a false alarm probability of 16% at peak maximum and 18% at the precise value of the rotation period. In the case of the survey data we found the single frequency false alarm probabilities (SFP) to deviate quite substantially from the theoretical $e^{-z}$ relation, so we also determined them via the bootstrap approach (see Appendix). We found them to be 0.40% (theoretical) and 0.076% (bootstrap) for the peak maximum and 0.47% (theoretical) and 0.089% (bootstrap) for the precise value of the rotation period. Table 2 summarizes these results.

For the first subset of the survey data we found the (semi-)amplitude of the best-fit sine wave with $P = P_{\rm rot}$ to be $1.24 \pm 0.31$ cts sec$^{-1}$. With a mean level of 6.487 cts sec$^{-1}$ this indicates rotational modulation of $\pm 19\%$.

## 5. Conclusions

AB Dor does not exhibit long-term variability of its coronal X-ray emission comparable to the extent observed in the Sun.

While we can certainly not exclude any cyclic (or irregular) variability of the coronal flux on time scales longer than our 5 1/2 years of ROSAT measurements we do not find any pronounced trend in AB Dor's average X-ray brightness in our data set, despite the fact that a high level of short-term variability is present. At best, a marginal increase of the X-ray flux may be inferred from the 5 1/2 years of ROSAT monitoring observations. This supports the concept of a saturated corona present in very active stars. AB Dor's 'saturated corona' must (at times) possess a partially inhomogeneous structure in order to be able to account for the $\pm(5-13)\%$ of geometrically induced short-term variability observed during the Oct/Nov 1991 pointing and the $\pm 19\%$ observed in the all-sky survey data (first subset).

In the time interval for which ROSAT data are available (mid-1990 to late 1995) also the V-band measurements show only a slight brightening of the star which has entered what appears to be a plateau in its long-term brightness trend. Certainly a longer time base for these correlated monitoring observations is needed before any conclusions about the relation between the long-term behaviour of the optical and X-ray fluxes are possible.

*Acknowledgements.* We thank A. Hatzes, K. Strassmeier, and S. Schaeidt for stimulating discussions. An anonymous referee made valuable suggestions for the improvement of the paper. The ROSAT project is supported by the German Bundesministerium für Bildung, Wissenschaft, Forschung und Technologie (BMBF/DARA) and the Max-Planck-Gesellschaft. MK acknowledges support by the Austrian Fond zur Förderung der wissenschaftlichen Forschung under grant S7302-AST.

## Appendix A: estimation of the significance of periodogram peaks via bootstrap

In our use of the Scargle periodogram (see Eq. 10 in Scargle 1982 for the definition) we follow largely the description given by Horne & Baliunas (1986). We are dealing here with two types of significance or probability estimates. One is the chance probability or false 'alarm probability' (FAP), the other is what we have named the 'single frequency false alarm probability' (SFP) in Sect. 4.1.2. While $1-FAP$ is the relevant estimator for the significance of a frequency in a *frequency search*, $1-SFP$ is the estimator for the significance of a signal at an *a priori known* frequency. Conversely, $FAP$ is the chance probability that a certain power is obtained at *some* frequency in the accessible frequency range from purely random data whereas $SFP$ is the chance probability that, at a *known* frequency, a signal is produced at random.

For normally distributed measurement errors

$$SFP = e^{-z} \tag{A1}$$

where $z$ is the correspoding power in the Scargle periodogram. The FAP is related to the SFP via

$$FAP = 1-(1-e^{-z})^{N_{\rm in}} \tag{A2}$$

where $N_{\rm in}$ is the number of independent frequencies in the data, a number that must be determined via a Monte Carlo simulation. Horne & Baliunas study the relation between the number of independent frequencies and the number of data points for different types of data sampling by producing (for a observed sampling pattern) a large number of random data sets having the same total variance as the observed data. They record the fraction of periodograms that contain a peak of a certain height or higher. By fitting eq. (A2) to the obtained cumulative distribution function of peak heights Horne & Baliunas determine the number of independent frequencies.

We are taking here a slightly different approach based on the bootstrap idea. Quite similar to our description of the trend analysis in the total monitoring data set for AB Dor (Sect. 3.2.2) we are using the observed distribution of count rates and observing times to come up with estimates for the SFP and the FAP (cf. Murdoch et al. 1993). Retaining the observing times and randomly redistributing the observed count rates amongst the times we ran 10,000 periodograms on the resulting randomized data sets and recorded

1. for each individual frequency: in what fraction of the periodograms a power at least as high as the power observed in the original periodogram was obtained;
2. the power of the highest peak in each periodogram.

From the first point the SFP can be estimated, whereas the false alarm probability for a frequency search can be determined from the second point. We found good agreement between the bootstrapped SFP and the theoretical SFP for small values of the power $z$; i.e. below about 2.5 for the survey data and about 5 for the pointing data. For higher values of $z$ the SFP become increasingly smaller than the theoretical values which then results in correspondingly smaller values of FAP for the high periodogram peaks. For a detailed discussion of the validity of the $e^{-z}$ behaviour of the power spectrum we refer the reader to the paper by Newman et al. (1982).

## References

Acton L.W.: 1996, 9th Cambridge Workshop, Cool Stars, Stellar Systems and the Sun, in press
Anders G.J.: 1994, IBVS 3985
Avni Y.: 197, ApJ 210, 642
Barrow J.D., Bhavsar S.P., Sonoda D.H.: 1984, MNRAS 210, 19p
Bieber J., Seckel D., Stanev T., Steigman G.: 1990, Nature 348, 407
Bos M.: 1994a, IBVS 4111
Bos M.: 1994b, Experimental Astronomy 5, 13
Bos M., Budding E., Hudson G., Hudson R.: 1995a, IBVS 4203
Bos M., Hudson G., Hudson R., Budding E.: 1995b, IBVS 4330
Cameron A.C., Bedford D.K., Ruciński S.M., Vilhu O., White N.E.: 1988, MNRAS 231, 131
Cutispoto G.: 1995, A&AS 111, 507
David L.P., Harnden F.R. Jr., Kearns K.E., Zombeck M.V.: 1993, The ROSAT High Resolution Imager (HRI), Technical Report, U.S. ROSAT Science Data center/SAO
Efron B.: 1979, Ann. Stat. 7, 1
Horne J.H., Baliunas S.L.: 1986, ApJ 302, 757
Innis J.L., Thompson K., Coates D.W.: 1986, MNRAS 223, 183
Innis J.L., Thompson K., Coates D.W., Lloyd Evans T.: 1988, MNRAS 235, 1411
Kürster M., Dennerl K.: 1993, Physics of Solar and Stellar Coronae, J. Linsky, S. Serio (eds.), Kluwer, p. 443

Kürster M., Schmitt J.H.M.M., Cutispoto G.: 1994, A&A 289, 899
Kürster M., Schmitt J.H.M.M., Fleming T.A.: 1992, 7th Cambridge Workshop, Cool Stars, Stellar systems and the Sun, M. Giampapa, J. Bookbinder (eds.), A.S.P. Conf. Ser. 26, p. 109.
Murdoch K.A., Hearnshaw J.B., Clark M.: 1993, ApJ 413, 349
Newman W.I., Haynes M.P., Terzian Y.T.: 1992, Statistical Challenges in Modern Astronomy, E.D. Feigelson, G.J. Babu (eds.), Spinger, p. 137
Pakull M.W.: 1981 A&A 104, 33
Pfeffermann E., et al.: 1987, Soft X-Ray Optics and Technology, SPIE Int. Soc. Opt. Eng. 733, 519
Ruciński S.M.: 1982, IBVS 2203
Ruciński S.M.: 1985, MNRAS 215, 591
Ruciński S.M., Mewe R., Kaastra J., Vilhu O., White S.M.: 1995, ApJ 449, 900
Scargle J.D.: 1982, ApJ 263, 835
Schmitt J.H.M.M.: 1985, ApJ 293, 178
Stauffer J.R., Caillault J.-P., Gagné M., Prosser C.F., Hartmann L.W.: 1994, ApJS 91, 625
Trümper J.: 1983, Adv. Space Res. 2, 241
Unruh Y.C., Collier Cameron A., Cutispoto G.: 1995, MNRAS 277, 1145
Vilhu O.: 1984, A&A 133, 117
Vilhu O., Linksy J.L.: 1987, PASP 99, 1071
Vilhu O., Gustafsson B., Edvardsson B.: 1987, ApJ 320, 850
Vilhu O., Tsuru T., Collier Cameron A., Budding E., Banks T., Slee E., Ehrenfreund P., Foing B.H.: 1993, A&A 278, 467
Vilhu O., Walter F.M.: 1987, ApJ 321, 958
White S.M., Pallavicini R., Lim J.: 1995, IAU Colloq. 151, Flares and Flashes, J. Greiner, H.W. Duerbeck, R.E. Gershberg (eds.), Lect. Notes in Phys. Ser., p. 168
Zimmermann H.U., Becker W., Belloni T., Döbereiner S., Izzo C., Kahabka P., Schwendtker O.: 1994, EXSAS User's GUIDE, MPE Report No. 257

This article was processed by the author using Springer-Verlag LaTeX A&A style file *L-AA* version 3.